A&A manuscript no.
(will be inserted by hand later)

Your thesaurus codes are:
09.11.1 – 11.11.1

ASTRONOMY
AND
ASTROPHYSICS
7.1.1998

Gas in Shearing Density Waves

Markus Demleitner

Astronomisches Rechen-Institut, Mönchhofstraße 12-14, 69120 Heidelberg, Germany

Received 4 September 97, accepted 24 November 1997

Abstract. We examine the development of a transient spiral arm in a disk galaxy made up of both gas and stars. To this end we have performed numerical simulations in a shearing sheet (basically a rectangular patch of a disc) that contains gas in the form of clouds behaving like Brahic's (1977) sticky particles, and stars that appear as a background continuum providing the perturbation forces. These are computed from the theory of swing amplification, using Fuchs' (1991) work. We describe the evolution of our model under a single and under recurring swing amplification events, discerning three phases. Furthermore, we give an interpretation of this evolution in terms of a variation of the epicyclic frequency with the distance to the wave crest. We also assess the importance of self gravity in the gas for our results.

Key words: Galaxies: kinematics and dynamics – ISM: kinematics and dynamics

1. Introduction

Since the work of Orr (1907) it has been known that certain perturbations in stable shearing flows show a transient exponential growth. This phenomenon was discussed extensively by Goldreich & Lynden-Bell (1965) and Julian & Toomre (1966) in the context of galactic dynamics, using hydrodynamics and statistical mechanics, respectively. Both papers examine the dynamics of a small patch within a larger disk and find strong transient growth of density perturbations as they "swing by" from leading to trailing. Toomre (1990) has argued that this amplification mechanism is the principal dynamical process responsible for spiral arms in disk galaxies.

While gas is known to play a major role in quasi-stationary density waves (Roberts 1969), there has been little research on the dynamical behavior of the interstellar medium (ISM) in transient density waves. It is this issue the present paper addresses. The key question we want to answer is whether the short lifetime of a swing-amplified perturbation still allows a noticeable response of the ISM. Additionally, we look for kinematical signatures that might allow a discrimination of quasi-stationary versus transient density waves.

So far, the only study of swing amplification in a two-component medium was undertaken by Jog (1992) who extended the formalism of Goldreich & Tremaine (1978) to include two fluids with different stability numbers. While these works used Lagrangian coordinates to solve the dynamical equations, in this paper we employ a different approach using Eulerian coordinates. This enables us to consider a succession of swing amplification events in a consistent way.

The outline of this paper is as follows: In section 2 we describe our model with a brief review of the results of Fuchs (1991) important to this work and a discussion of our treatment of an ISM consisting of discrete clouds. Section 3 presents the main results. In a first part, we describe the behavior of our model under a single perturbation. This behavior is interpreted in the second part. After a discussion of the model with repeated perturbations, section 3 closes with an investigation of the effects of self gravity in the ISM. In Section 4 we briefly summarize the main conclusions we draw from this work.

2. The Model

Due to the inherently local nature of swing amplification no global disk model is required. Instead, we use a sliding box scheme similar to the one used by Toomre & Kalnajs (1991). The central idea of the sliding box scheme is to examine the dynamics of a rectangular patch of a galactic disk that is periodically repeated such that when, for example, a particle leaves the patch at the rotationally leading border, it is re-fed at the trailing one. This resembles the periodic boundary conditions used in plasma and solid state physics, with the complication that in galactic dynamics the periodic continuations must share the general shear of the disk. In consequence, particles leaving the patch radially must be re-fed at the opposite edge at positions varying with time, and the difference in circular velocities between the inner and outer edges must be accounted for, so as to keep the accelerations continuous during the re-feeding process.

In such a patch pseudo-Cartesian coordinates $x = r - r_0$ and $y = r_0(\vartheta - \Omega_0 t)$ are introduced, where r, ϑ are galactocentric polar coordinates, r_0 is the distance of the center of the patch from the center of the galaxy, Ω_0 is the angular velocity at r_0, and t denotes the time. After inserting these new coordinates into the equations of motion derived from the Lagrangian $L = \frac{1}{2}(\dot{r}^2 + r^2\dot{\vartheta}^2) + \Psi(r, \vartheta)$ with the potential $\Psi(r, \vartheta)$, we linearize the equations with respect to x and y. The linearization is valid under the assumption that (a) the radial extent of the patch is small compared to the scales over which the basic state of the galaxy varies significantly and (b) the peculiar motions are much smaller than the circular velocities. Note that no assumption about the circumferential extent of the patch is necessary.

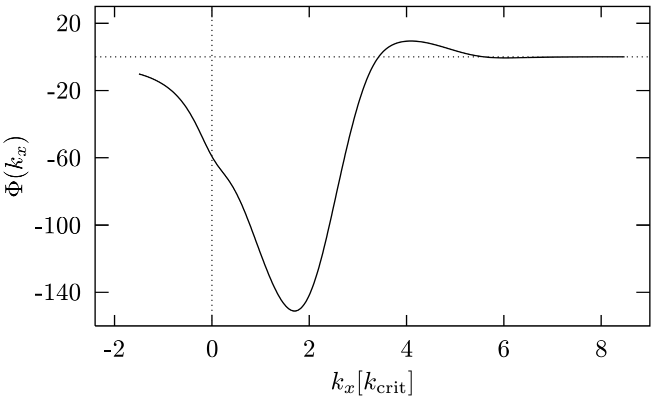

Fig. 1. Amplitude of the potential perturbation, given in arbitrary units. The initial amplitude of the potential perturbation at $k_x = -1.5k_{\rm crit}$ and the minimum at about $k_x = 1.6k_{\rm crit}$ correspond to density perturbations of roughly $0.006\Sigma_0$ and $0.1\Sigma_0$ amplitude, respectively. Since the radial wave number increases linearly with time, this also shows the temporal development of the wave. The interval of wave numbers shown here, $k_x = -1.5 \cdots 8\,k_{\rm crit}$, corresponds to a time interval of 7×10^8 years.

This leads to the epicyclic equations of motion

$$\ddot{x} = 2\Omega_0\dot{y} + 4\Omega_0 A_0 x + f_x \qquad (1a)$$

$$\ddot{y} = f_y - 2\dot{x}\Omega_0, \qquad (1b)$$

where f_x, f_y are the acceleration components due to the spiral field. A_0 denotes Oort's first constant. The perturbation forces are calculated according to the work of Fuchs (1991) where the Boltzmann and Poisson equations were used to obtain the perturbation potential in the form

$$\Phi(x, y; t) = \Phi_0(t)\exp\bigl(\mathrm{i}\boldsymbol{k}\cdot\boldsymbol{r}\bigr), \qquad (2)$$

where $\boldsymbol{k} = \bigl(k_x(t), k_y\bigr)$ is the wave vector of the perturbation. Since swing amplification is most effective in the vicinity of $k_y = 0.5\,k_{\rm crit}$, we use this choice throughout the following. In the case of free swing amplification one has $k_x(t) = k_x^{\rm in} + 2k_y A_0 t$ for a sinusoidal excitation with an initial radial wave number $k_x^{\rm in}$ and assuming positive k_y. While one has to expect that excitations will not be sinusoidal in reality, the restriction to a single Fourier component should not be critical due to the linearity assumed in the derivation of Eq. (2) and because components with wave numbers significantly different from an optimal $k_x^{\rm in}$ will either be not amplified strongly or damped out before reaching the zone of amplification.

The integral equation determining the amplitude function $\Phi_0(t)$ derived by Fuchs (1991) is solved numerically. Its solution is shown in Fig. 1 for the standard parameters of our model,

$$\begin{array}{ll} k_{\rm crit} = 2\pi/(10\,{\rm kpc}) & A_0 = 0.015\,{\rm km\,s^{-1}\,pc^{-1}} \\ k_x^{\rm in} = -1.5\,k_{\rm crit} & B_0 = -0.01\,{\rm km\,s^{-1}\,pc^{-1}} \\ Q^2 = 2 & \mu^{\rm in}/\Sigma_0 = 1/(50\pi), \end{array}$$

where $k_{\rm crit} = \kappa^2/2\pi{\rm G}\Sigma_0$ is Toomre's critical wave number, defined with the epicyclic frequency κ, the gravitational constant G and the unperturbed mass surface density Σ_0. Our choice of $k_{\rm crit}$ gives $\Sigma_0 = 58\,M_\odot\,{\rm pc}^{-2}$, somewhat more than what is found for the Milky Way in the solar neighbourhood (Kuiken & Gilmore 1991). Q is the Toomre stability parameter, $\mu^{\rm in}$ is the amplitude of the initial density perturbation, and B_0 denotes Oort's second constant. With these parameters one has $\Omega_0 = 0.025\,{\rm km\,s^{-1}\,pc^{-1}}$ with a locally slightly falling rotation curve. The only assumption about the distance to the center of the disk is $\Omega_0 r_0 \gg \sigma$. While the choice of $k_{\rm crit}$, A_0, B_0, and Q is not meant to accurately model the solar neighborhood, we regard it as representative for the outer regions of giant spirals. Our results are generic in that they do not qualitatively change under reasonable modifications of these parameters. For example, as long as $-B_0$ is comparable to A_0, it is unimportant whether the rotation curve is flat, rising or falling.

Equation (2) describes sinusoidal waves of constant circumferential wavelength. Due to the shear of the disk, the radial wavenumber k_x grows with time. In this way an initially leading wave ($k_x^{\rm in} < 0$) is transformed into a trailing one and, as can be seen in Fig. 1, strongly amplified while "swinging by". With increasing k_x phase mixing leads to a damping of the perturbation as the wavelength of Φ drops beyond the typical epicycle size. A single swing amplification event from excitation to decay has a duration of a few 10^8 years.

In our model the ISM is approximated as a dissipative medium of discrete clouds. Their motions are governed by equations (1) as long as they do not collide. Collision detection is performed on a grid of width $R_{\rm coll}$, where we chose $R_{\rm coll} = 50\,{\rm pc}$. If there are two or more clouds in one cell, we form pairs by a random process and let a pair collide if the clouds that make it up are approaching each other. The collisions treat clouds as "sticky" spheres, i.e. their relative velocities are multiplied by a factor $(1 - f)$ after performing an elastic two-body collision (Brahic 1977, Schwarz 1981). In such a system the cooling rate depends on the collision rate and the inelasticy coefficient f. To have a clear signature of the collisonal nature of the cloudy medium, we have selected a high collision rate (about $0.2\,\mathrm{step}^{-1}$) which in turn requires a comparatively low f of 0.2 to prevent the system from cooling down too quickly. For the implication of this choice, see the comprehensive investigation by Jungwiert & Palous (1996). However, as long as the total cooling rate is kept constant, our model is much less sensitive to the choice of f than theirs. With these parameters, an unperturbed system of clouds with Gaussian velocity distribution cools down exponentially with a characteristic time of about 200 Myr. Collisions are checked for once every step, where one time step equals $3\,\mathrm{pc\,s\,km}^{-1}$.

The sticky particles are initially homogeneously distributed with a density of $0.0003\,\mathrm{pc}^{-2}$ and have a Gaussian velocity distribution. We chose a radial velocity dispersion of $\sigma_u \approx 4.2\,\mathrm{km\,s}^{-1}$. The velocity dispersion in the y-direction was set according to the epicyclic ratio $(2\Omega_0/\kappa)$, resulting in a total initial velocity dispersion of $\sigma = 5\,\mathrm{km\,s}^{-1}$. As long as $\sigma(t = 0)$ is low enough (say, $< 10\,\mathrm{km\,s}^{-1}$), the behaviour of the model is not strongly influenced by this choice.

Velocity dispersions of this order are typical of giant molecular clouds (Clemens 1985). Our sticky particles, however, are not meant to mimic GMCs themselves. Their number is much larger than that of GMCs, they are stable, and of course their dynamical behavior can at best be regarded as idealized from real clouds. Technically, they just implement a dissipative medium. From the structure of the equations of motion, we do not need to make any assumptions about the masses of the clouds. Also, it is very hard to assign radii to the model clouds from the sticky particles formalism. One might use $R_{\mathrm{coll}}/2$ as a gross measure of the collision cross section. The details of the modeling do not seem to be critical for our results, since the dissipativity of the medium does not influence its dynamical evolution very significantly except through cooling (see below). In this way, our results would be largely unchanged if, for example, one increased f and lowered the initial density accordingly to keep the collision rate constant.

Introducing two-particle interactions like collisions requires some care in strictly two-dimensional calculations like the present one. Rybicki (1972) showed that in contrast to three-dimensional systems in two-dimensional self-gravitating sheets the relaxation time is always of the order of the crossing time. Interactions "softer" than gravity are, however, less affected by this limitation. In fact, one can choose $T_{\mathrm{relax}}/T_{\mathrm{crossing}}$ of the ISM freely in our model by changing R_{coll} and the initial surface density since all interactions with impact parameters smaller than R_{coll} are equivalent. Checks with 3-D-models showed no significant deviations from the evolution described below.

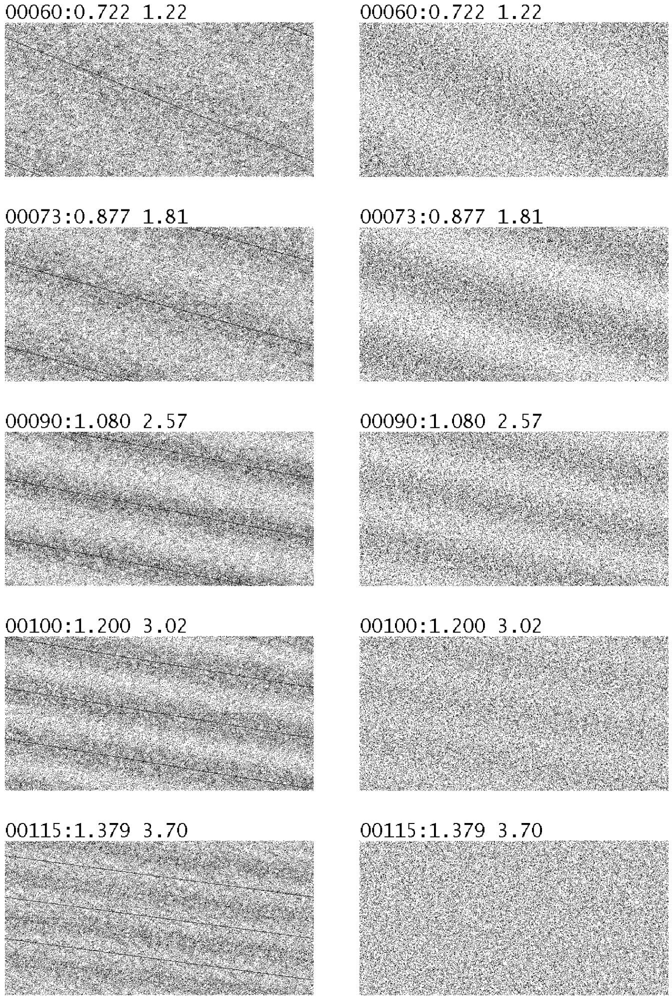

Fig. 2. The distribution of gas clouds (left) and "backbone" stars (right) in a patch of dimensions $20\,\mathrm{kpc} \times 10\,\mathrm{kpc}$, giving 60000 clouds in the patch. The radial direction is upwards and the galactic rotation towards the right. Above each panel the step number, the time since the excitation in units of galactic rotations (given for illustrative purposes only and computed for an assumed $r_0 = 8\,\mathrm{kpc}$) and the k_x of the perturbation in units of k_{crit} are indicated. In the frames on the left each dot represents a gas cloud and the straight lines mark phases zero and $\pm 2\pi$ of the shearing wave. The frames on the right side are scatter plots of the surface density $\Sigma(x, y)$ obtained from inserting (2) into the Poisson equation. To make the structures in the stellar disk visible, we enhanced the contrast in the stellar density by a factor of four.

3. Results

3.1. Evolution of a Single Density Perturbation

In Fig. 2 we show the spatial distributions of clouds and stars in a patch of a galactic disk constructed in the way

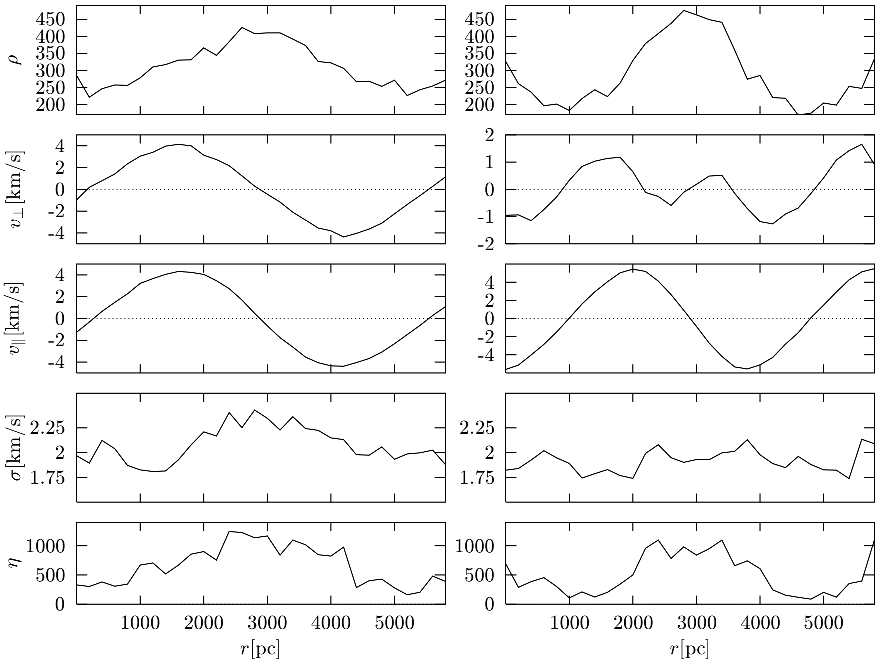

Fig. 3. Profiles of the density ρ, the streaming velocities perpendicular and parallel to the the wave crest after subtracting the basic shear, $v_\perp$ and $v_\parallel$, and the velocity dispersion, σ, in $\mathrm{km\,s^{-1}}$ across a spiral arm, and the energy dissipated in collisions per unit time and area, again in arbitrary units. The profiles on the left have been taken at step 73 and illustrate the state of the patch during a formation phase of the spiral arms. On the right we illustrate the onset of the dissolution phase with profiles taken at step 90. These profiles were obtained along lines of 6 kpc length perpendicular to the density wave crest. The wave crest is at $r = 3\,\mathrm{kpc}$.

described above. We chose a rather large radial extent of the patch, $b_x = 10\,\mathrm{kpc}$, in order to give a clear impression of what is going on. The physical relevance of the upper and lower edges of the displayed patch may therefore be doubtful, whereas in the region around $x = 0$, located in the center of each frame, the linearization performed above is well justified.

The first frame in the series shows the state of the patch about three quarters of a galactic rotation after the perturbation has been excited. The perturbation is already trailing and well developed in the galaxy's stellar "backbone" on the right. The gas has responded to the potential perturbation and the amplitude of the density perturbation in the gas is comparable to the one in the stars.

This changes about 30 Myr later, when the arm-interarm density contrast in the stars has just passed its maximum of about 1.4:1. As can be seen from Fig. 3 the density contrast in the gas is almost 2:1 at this stage. The flow pattern is characterized by an inflow towards the wave crest and a tangential flow that transports clouds inwards on the outer edge of the arm and outwards on the inner edge. Judging from the sinusoidal profiles, we still are in the linear regime. These profiles resemble analogous results from simulations with discrete clouds in quasistationary density waves (the results of Roberts (1992) are particularly well suited for comparison). The main difference is that shearing density waves are essentially at rest with respect to the disk material around them and thus produce structures symmetric to the wave crest, whereas stationary density waves outside the corotation zone have an upstream and downstream side and thus lead to asymmetric profiles.

While the perturbation amplitude in the stars declines from now on (cf. Fig. 1), the spiral arm in the gas continues to grow for another 50 Myr, as seen in the third frame in Fig. 2. With this maximal density contrast in the gas, the formation phase of the spiral arm comes to an end. The following dissolution phase is marked by a gradual turnover from inflow to outflow with respect to the wave crest. In the velocity component perpendicular to the wave crest, $v_\perp$, a double-wave pattern evolves (cf. Fig. 3).

As can be seen in the fourth frame in Fig. 2, the spiral arms widen during the dissolution phase, and their edges sharpen. This shift of activity towards the edges is discernible in the σ-profile shown in Fig. 3, right side, where one already has maxima at the arm's edges. At this stage hardly any perturbation is visible in the stellar disk.

In the last frame shown in Fig. 2, taken about half an epicyclic period after the strongest expression of the pattern, the gas clouds once more gather into a density concentration, this time at phases $\pm(2j+1)\pi$, $j \in \mathbb{N}$, of the original density perturbation. Apart from the shift in phase and the smaller wavelength, profiles in ρ, $v_\perp$, and $v_\parallel$ across this "echo" arm closely resemble those given in Fig. 3, left column. However, it has no visible counterpart in the stellar disk. Another half epicyclic period later one again finds an echo, this time with maxima at the positions of those of the original density perturbation. These echoes are only slowly damped out.

3.2. Physical Interpretation

To get an understanding of the dynamics of the patch, it is advantageous to introduce the crest distance in units of the perturbation wave length, $\tilde{r}(t) = \boldsymbol{rk}/(2\pi)$. In $\tilde{r}$ unperturbed circular orbits appear as parallels to the x-axis, and

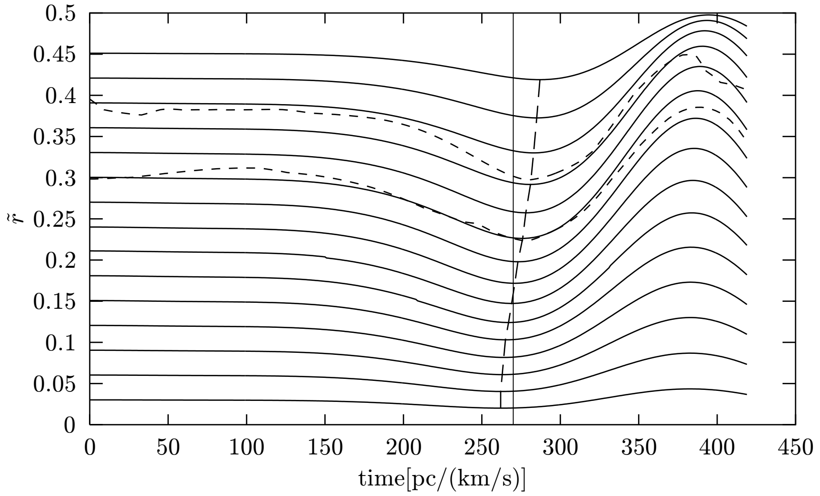

Fig. 5. Time evolution of crest distances. Here we show the distances of 15 collisionless particles starting with zero peculiar velocity (solid lines) in units of the time-dependent wavelength of the potential perturbation. The long-dashed line connects the epochs of the turnover of the particles' motion, and the vertical line marks the time at which the profiles on the right hand side of Fig. 3 were taken. The short-dashed lines indicate crest distances of two gas clouds from our reference simulation for comparison. Note that $\lambda(t)$ varies between 20 kpc and 2 kpc in the time interval shown in this diagram, hence the amplitude of the oscillation is no measure for the sizes of the epicycles.

the acceleration due to the perturbation is always parallel to the measuring rod. The drawback is that the length unit varies with time, so that orbits of constant nonzero epicyclic amplitude appear to have growing amplitude in $\tilde{r}$ when $k_x > 0$.

The evolution of $\tilde{r}(t)$ for 15 particles moving in our reference model without collisions is shown in Fig. 5. The particles start on circular orbits and are accelerated towards the wave crest for the first $200\,\mathrm{pc\,s\,km^{-1}}$, indicated by a negative curvature in $\tilde{r}(t)$. At about the time when the stellar arm starts to dissolve ($k_x \approx 1.7\,k_{\rm crit}$ by Fig. 1, corresponding to $t \approx 210\,\mathrm{pc\,s\,km^{-1}}$), the curvature changes sign. The net force on a particle must therefore be directed away from the wave crest, although $\Phi_0(t)$ is still negative. This is because the Coriolis force present in the equations of motion (1) is now stronger than the perturbation force. While the latter decays, the Coriolis force finally turns around the motion. Since the relative strengths of perturbation and Coriolis forces vary with the crest distance, the epoch of this turnover also depends on $\tilde{r}$. This delay in turnover time causes the double wave shown in Fig. 3 on the right side.

While it is possible to gain a qualitative understanding of the variation of turnover times in terms of the ratio of perturbation versus Coriolis force, the problem is better understood in terms of a perturbation of the epicyclic frequency, i.e. by letting the angular frequency of a supposed periodic motion in a shearing reference frame vary with the distance to the wave crest. For a simplified version of the present potential, we derive

$$\frac{\tilde{\kappa}^2(r)}{\kappa^2} \approx \left(1 - \frac{k\alpha}{\kappa^2}\cos(kr)\right) \tag{3}$$

in the appendix for the perturbed epicyclic frequency $\tilde{\kappa}$ where α is the amplitude of the perturbation—which is negative during the formation phase—, k is its wave number and r denotes the distance from the wave crest. Thus, the double wave is a consequence of $\tilde{\kappa}$ increasing towards

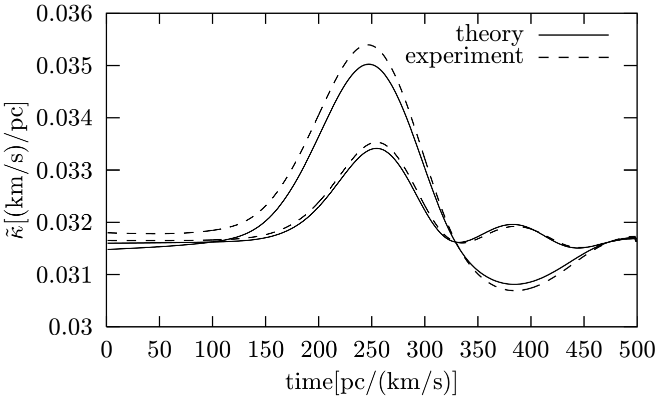

Fig. 4. Perturbed epicyclic frequencies $\tilde{\kappa}$ for two distances from the wave crest as a function of time. The solid lines are computed from Eq. (3). The dashed lines are averages for the epicyclic frequencies over the numerically integrated orbits of 250 particles distributed evenly on an epicycle with $u = 10\,\mathrm{km\,s^{-1}}$. For the upper curve, the guiding center of the epicycle lies at $x = 200$ kpc, for the lower curve at $x = 1500$ kpc.

the wave crest. As can be seen from Fig. 4, the rough estimate Eq. (3) already is quite a good approximation to the more complex situation in our simulation.

Fig. 5 also shows how the dissolution phase turns over into the formation of the echo arm as the clouds proceed on their epicycles. After $t = 300$ Myr ($k_x = 3\,k_{\rm crit}$, cf. Fig. 1) the potential perturbation is practically zero, and therefore the echoes simply are kinematical spiral arms (Kalnajs 1971). They do not appear in the stellar disk because of the much higher velocity dispersion of the stars. For our choice of $k_y = 0.5\,k_{\rm crit}$, the size of the stellar epicycles gets comparable to the perturbation wavelength shortly after the maximal amplification, and phase mixing leads to an exponential damping. Thus the only sign of kinematical spiral arms in the backbone stars is a small overshoot of Φ_0 around $k_x = 4\,k_{\rm crit}$ (cf. Fig. 1).

In contrast, the echo arm in the gas has about the amplitude of the primary spiral arm. This is mainly because of the smaller velocity dispersion of the gas. When phase mixing becomes important in the stars, the wave length of the perturbation is still much larger than the typical size of an epicycle of a cloud. Only at a wavelength of about 500 pc ($t > 900$ Myr) does phase mixing dominate the damping of the perturbation in the gas. Until then, the perturbation is mainly damped by collisions that are not very efficient in damping away larger-scale structures. Thus, even when radial variations of κ weaken the kinematical spiral arm, at least the first echo can be expected to be reasonably strong. One might speculate that echoes of this kind have some relation to "gaseous interarms", spiral arms in the ISM without corresponding activity in the stellar disk (e.g., Block et al (1994), although their observations only cover spirals with much higher density amplitudes than we consider here).

The discussion of the dynamical evolution of the patch given so far did not make any reference to the dissipativity of the cloudy medium. In fact, turning collisions off does not strongly change the evolution of the density perturbation in the ISM. The impact of the dissipativity on the dynamics is small because the streaming motions induced by the perturbation are quite smooth, so that the dissipativity of the medium mainly appears as viscosity that can be disregarded on short time scales. On longer time scales, however, the dissipativity of the cloudy medium keeps its velocity dispersion low, whereas a single swing amplification event roughly doubles the temperature of a stellar system with $\sigma(t = 0) = 5\,\mathrm{km\,s^{-1}}$.

Spiral arms are traced by young stars and HII-regions. Although the question has been under some debate (Elmegreen & Elmegreen 1986), it appears that density waves do modulate either the initial mass function or the star formation rate nonlinearly (Cepa & Beckman 1990). Kwan & Valdes (1983) have argued that massive star formation is triggered by collisions between diffuse molecular clouds. Following this line one might expect the energy dissipated in collisions per unit time and area, η, to give a coarse measure for the efficiency of massive star formation. Though this is a naïve view of how star formation proceeds in molecular clouds, the compression induced by the development of spiral arms certainly plays a role in triggering the collapse of molecular clouds and hence star formation. As can be seen from Fig. 3 we find contrasts in η of up to $1 : 10$ from arm to inter-arm regions since η is larger in the arms.

3.3. Consecutive Swing Amplification Events

Certainly the processes investigated here will not take place only once for each galaxy; instead, we expect excitations to recur in a more or less stochastic manner. To examine the behavior of the patch under repeated perturbations, we need to make some assumptions regarding the frequency and the amplitude spectrum of the amplification seeds. In our model, we are rather limited in the first of these choices because the crests of the density waves must always connect the centers of adjacent patches to keep the perturbation potential continuous across patch borders. Consequently, the swing amplification events must follow one another with a period of $b_y/(2A_0 b_x)$ (or a multiple thereof), where the circumferential extent of the patch is already fixed to $b_y = 2\pi/k_y$ by the continuity condition across circumferentially adjacent patches.

In contrast, we expect swing amplification events to follow one another in a more or less random fashion. This should be the case for seeds provided by Poisson noise or massive perturbers of the disk (Toomre 1990). Even recurrent swing amplification due to mode coupling as studied by Fuchs (1991) will have a stochastic nature. Thus strictly periodic excitations are probably grossly unphysical. However, as neither the global kinematics nor the overall morphology of the patch strongly depends on the excitation period as long as one avoids resonances with the epicyclic period, one can still gain some insight in the long term evolution of the patch. For simplicity, we use the same amplitude for all seeds.

The general appearance of the patch subjected to such repeated perturbations qualitatively resembles the sequence shown in Fig. 2 for a single swing amplification event. However, the spiral arms are more ragged with crossings and bridges, because the potential perturbations act on a disk that is already structured both in density and velocity. For excitation periods used here, only one swing amplification event causes noticable perturbation forces at any moment. This corresponds to the fact that the lifetime of any perturbation will be much shorter in the backbone stars with their high velocity dispersion than in the cool cloudy medium. One consequence of this is that the spiral arm in the backbone stars will be much smoother than in the cloudy medium with no crossings and bridges appearing. Again, this invites comparison with the observations of Block et al (1994), who see much smoother arm shapes in the infrared than in the optical.

In longer-term simulations the gas reaches a quasi-equilibrium state after the first few excitations. Then, the global velocity dispersion including streaming motions oscillates by about $1\,\mathrm{km\,s^{-1}}$ around a mean value of about $\sigma \approx 6\,\mathrm{km\,s^{-1}}$ for our parameters. This mean value increases slightly with decreasing τ_e over a range of excitation periods from $150\,\mathrm{pc\,s\,km^{-1}}$ to $400\,\mathrm{pc\,s\,km^{-1}}$ (excluding resonances with κ). This equilibrium is remarkably independent of the collision parameters. Going from a mean collision rate of $0.14\,\mathrm{step^{-1}}$ to $0.3\,\mathrm{step^{-1}}$ one finds the temporal mean of the velocity dispersion decreases by less than $0.25\,\mathrm{km\,s^{-1}}$, where most of the difference is due to the systems with high collision rates cooling down more quickly from a peak velocity dispersion of about $6.5\,\mathrm{km\,s^{-1}}$ that is almost independent of the collision rate.

The reason for this behaviour is that in the later evolution σ is dominated by the thermalization of streaming motions. These are to zeroeth order independent of the velocity dispersion before the swing amplification event. Thus, cool systems are heated to the about the same temperature as warmer ones. As long as the system is able to cool down between two swing amplification events, and provided that the streaming motions are not destroyed by too frequent collisions, the sole difference between the cooler and warmer systems lies in the the amplitude of the temperature oscillations. Only when collisions become unimportant—at collision rates of, say, $0.05\,\mathrm{step}^{-1}$—, does this reasoning break down and the mean velocity dispersion rises to values of the order of $10\,\mathrm{km\,s}^{-1}$. The velocity dispersion of a collection of collisionless test particles in the perturbed disk rises to about $20\,\mathrm{km\,s}^{-1}$ within 3 Gyr, which is still much less than the $45\,\mathrm{km\,s}^{-1}$ of a stellar disk with the values of Q and Σ_0 we assume.

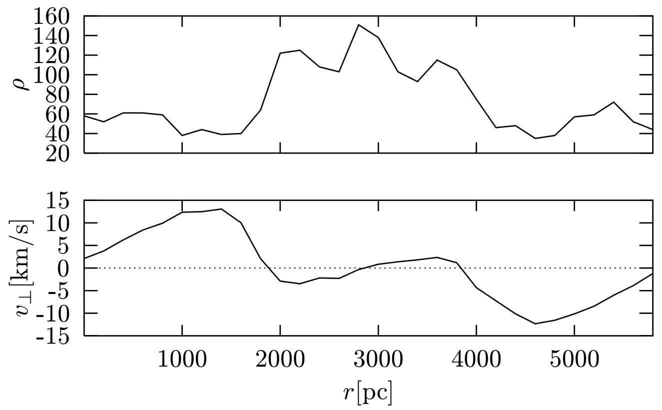

Fig. 6. Profiles of ρ and $v_\perp$ analogous to the ones shown in Fig. 3, this time taken after 1.5 Gyr of evolution under consecutive swing amplification events.

The profiles in Fig. 6 show that by constructive interference between two swing amplification events a prestructured ISM can show a much more vigorous response to a perturbation than the homogeneous patch examined above. Of course, destructive interference also occurs. Finding profiles like the one shown in Fig. 6 should be quite within reach of current observational techniques.

One also finds that the double-wave pattern can persist for up to 1/3 of the lifetime of a spiral arm, depending on how the excitations follow one another.

3.4. Self gravity

Jog (1992) predicts from her two-fluids model that the oscillation frequency for spiral arms in the gas is much lower than for the stars from a self-consistent two-fluid model. This is not the case in our cloudy medium. In fact, kinematical spiral arms in an ISM consisting of massless clouds will oscillate with the epicyclic frequency. The question arising naturally is whether the oscillation frequencies in gas and stars are so similar because of the neglect of self gravity in the ISM.

The investigation of the effects of self gravity could be implemented by a straightforward N-body code for our discrete clouds. However, considering Fig. 2 one notices that the density evolution in the gas has the form of a shearing wave that closely follows the evolution of the stellar perturbation in wavelength and inclination. Thus the additional perturbation potential arising from the gas clouds can be taken into account by assuming that the surface density of the gas sheet is modulated like $\mu_{\mathrm{gas}} \propto \exp(i\boldsymbol{k}\cdot\boldsymbol{r})$ with $\boldsymbol{k} = (k_x^{\mathrm{in}} + 2A_0k_yt, k_y)$.

Assuming a linear response the Poisson equation yields the additional potential perturbation arising from self gravity

$$\Phi_{\mathrm{self}}(x,y;t) = K\frac{|\boldsymbol{k}^{\mathrm{in}}|}{|\boldsymbol{k}(t)|}\frac{\epsilon\Sigma_0}{\mu^{\mathrm{in}}}\Phi_0(k_x^{\mathrm{in}})\cos(\boldsymbol{k}\cdot\boldsymbol{r}), \tag{4}$$

where $\boldsymbol{k}^{\mathrm{in}}$ denotes the wave vector of the initial perturbation, $\epsilon = \mu_{\mathrm{gas}}/\mu_{\mathrm{stars}}$ and K is the Fourier amplitude of the perturbation in the gas on $\cos(\boldsymbol{kr})$. In practice, K is determined by a least-squares fit of $K\cos(\boldsymbol{k}\cdot\boldsymbol{r}) + \bar{\mu}$ to a density cut perpendicular to the wave crest.

The assumption of a linear response is certainly valid in the early stages of the evolution, while its justification is somewhat doubtful for the later stages of the dissolution phase when the edges of the arm get very sharp. Still, one may expect results that allow a qualitative judgment on the importance of self gravity.

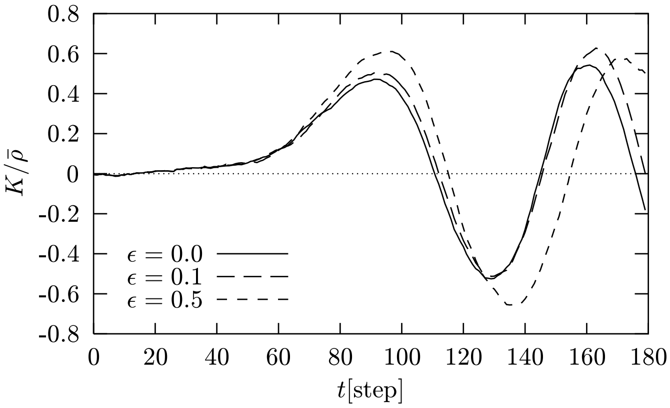

Fig. 7. Time evolution of the density contrast of the spiral arm for three values of the gas-to-stars mass ratio. For a low gas mass fraction, the effect of self gravity is negligible.

Figure 7 shows that neglecting self gravity is well justified in our model for gas mass fractions similar to those found in the solar neighborhood; the oscillation frequency of the arm in the gas does not change much for $\epsilon = 0.1$. For late-type spirals with a high gas content, however, self gravity alters the behavior significantly and our results should be applied with care. In particular, looking at profiles analogous to Fig. 3 one finds that a higher gas mass fraction will lead to softer edges and a less pronounced double wave during the dissolution phase.

Of course, this scheme, being designed to assess the consequences of neglecting self gravity on the large scale evolution in our two dimensional sheet, cannot describe many effects certainly important to disk evolution. In particular, Toomre (1990) pointed out that an N-body simulation in a patch similar to ours rapidly develops GMC-like complexes that might act as seeds for swing amplification. One can expect these to occur as well in the cloudy medium investigated here if it were fully self gravitating. However, an examination of these processes, possibly leading to self-triggered swing amplification with gas coupling back on the stars, is beyond the scope of this paper.

4. Conclusion

In this work we used a model consisting of a stellar continuum and gas clouds behaving like sticky particles to examine the behavior of gas in transient density waves. In contrast to the prior work of Jog (1992) that employed a gas-dynamical approach we find that the evolution of the density perturbation in the gas remains closely coupled to the one in the stars even when self gravity of the ISM is taken into account.

In a first phase, the ISM responds to the growing potential perturbation by flowing towards the wave crest. When the potential perturbation already decreases, the amplitude in the gas continues to grow until the dissolution of the gaseous arm begins due to Coriolis forces. In this process, a variation of a cloud's epicyclic frequency with its distance from the wave crest leads to a double wave in the velocity perpendicular to the arm, with particles near the wave crest already flowing outward while those further out are still moving in. We regard this as a strong signature for transient density waves that might be within reach of current observational techniques. Finally, the gaseous arms continue to evolve as kinematical spiral arms until they are finally damped out by phase mixing.

For the longer-term evolution we propose that swing amplification events follow one another in a more or less random fashion. We find that for a wide range of excitation frequencies spiral arms continue to form and dissolve. By interference between density waves a ragged morphology results. The dissipativity of the gas—unimportant for the short-term dynamics—keeps the velocity dispersion of the clouds low and thus their responsiveness high.

Given the stochastic nature of the processes described here, one cannot predict the appearance of a galaxy based on a knowledge of its basic state using the methods applied in this work. However, since our results are quite insensitive to the choice of parameters of the underlying model, we regard them as fairly generic for transient density waves. Thus, finding a double wave in radial velocity in the line of sight across a spiral arm for some component of low velocity dispersion (e.g., gas or OB-associations) would make a strong point for the existence of transient spiral arms.

Acknowledgements. I gratefully thank B. Fuchs and R. Wielen for many helpful discussions and encouragement during the course of this work. The comments of the referee M. Gerin helped to improve the presentation of the model and the results.

References

Bertin G., Lin C.C., Lowe S.A., Thurstans R.P., 1989, ApJ 338, 78
Block D.L., Bertin G, Stockton A, Grosbøl P, Moorwood A.F.M., Peletier R.F., 1994, A&A 288, 365
Bogoliubov N.N., Mitropolski Y.A. 1961: Asymptotic Methods in the Theory of Non-Linear Oscillations, Gordon&Breach, New York
Brahic A., 1977, A&A 54, 895
Cepa J., Beckman, J.E., 1990, ApJ 349, 497
Clemens D.P., 1985, ApJ 295, 422
Elmegreen, B.G., Elmegreen, M.E., 1986, ApJ 311, 554
Fuchs B., 1991, In: Sundelius B. (Ed.), Dynamics of Disk Galaxies, Göteborg University, Göteborg, p. 359
Goldreich P., Lynden-Bell D., 1965, MNRAS 130, 125
Goldreich P., Tremaine S., 1978, ApJ 222, 850
Jog C.S., 1992: ApJ 390, 378
Julian W.H., Toomre A., 1966, ApJ 146, 810
Jungwiert B., Palous J., 1996, A&A 311, 397
Kalnajs A., 1971, ApJ 166, 275
Kuijken K., Gilmore G., 1991, ApJ 367, L9
Kwan J., Valdes F., 1983, ApJ 271, 604
Orr W., 1907, Proc. Roy. Irish Acad. **A27**, 69
Roberts W.W., Jr., 1969, ApJ 158, 123
Roberts W.W. Jr., 1992, In: Dermott S.F., Hunter J.H., Wilson R.E. (Eds.): Astrophysical Disks, New York, p. 93
Rybicki G., 1972, In: Lecar M. (Ed.), Gravitational N-Body Problem (Proceedings of the tenth IAU-Colloquium), Reidel, Dordrecht, p. 22
Schwarz M.P., 1981, ApJ 247, 77
Toomre A. 1964: ApJ 139, 1218
Toomre A., 1990, In: Wielen R. (Ed.), Dynamics and Interactions of Galaxies, Springer, Berlin, Heidelberg, New York, p. 292
Toomre A., Kalnajs A. 1991, in Sundelius B. (Eds.), Dynamics of Disk Galaxies, Göteborg University, Göteborg, p. 339

Appendix

In the special case of a weak and purely radial perturbation, $(f_x, f_y) = (\alpha \sin(kx), 0)$, it is easy to show the dependence of the local oscillation frequency on the position of the particle within the density wave. While this is quite different from the potential arising from a shearing density wave, one can readily verify by numerical integration of the orbits that the oscillation frequency of mass points in a potential of the type of Eq. (2) roughly follows the behaviour predicted here with minor deviations resulting from the time-dependence of the wavelength of the perturbation (Fig. 4).

The assumption of a purely radial perturbation allows a closed integration of Eq. (1b). Inserting the result into Eq. (1a) yields

$$\ddot{x} = 2\Omega v_0 - \kappa^2 x + \alpha \sin(kx), \tag{A1}$$

where v_0 is an integration constant. To the author's knowledge, a closed solution of this differential equation does not exist. We therefore chose to investigate its solutions using the method of harmonic balance (e.g., Bogoliubov & Mitropolski 1961). We assume a quasi-harmonic solution of the form

$$x(t) = x_0 + x_1 \sin(\tilde{\kappa} t),$$

where $\tilde{\kappa} = \tilde{\kappa}(x_0, x_1)$. Inserting this into Eq. (A1) and Fourier analyzing the nonlinear term leads to

$$\begin{aligned} -\tilde{\kappa}^2 x_1 \sin(\tilde{\kappa} t) = {} & \kappa^2 x_0 - 2\Omega_0 v_0 + \alpha \sin(kx_x) J_0(kx_1) \\ & + \left(\kappa^2 - \frac{2\alpha}{x_1} \cos(kx_0) J_1(kx_1)\right) x_1 \sin(\tilde{\kappa} t) \quad \text{(A2)} \\ & + \text{higher Fourier components,} \end{aligned}$$

where J_0 and J_1 denote the Bessel functions of order 0 and 1, respectively. By comparing the 'leading' terms proportional to $\sin(\tilde{\kappa} t)$ one obtains

$$\tilde{\kappa}^2 = \kappa^2 \left(1 - \frac{2\alpha}{\kappa^2 x_1} J_1(kx_1) \cos(kx_0)\right). \tag{A3}$$

A straightforward application of (A3) to the perturbation used in our simulations—justified *a posteriori* by Fig. 4—can be done by identifying x_0 with the distance of the guiding center of a particle from the wave crest. Since the epicycle sizes are small compared to the wavelegth $2\pi/k$ of the perturbation, one may furthermore approximate $J_1(kx_1)/x_1 \approx k/2$. This leads to Eq. (3). These approximations obviously break down for epicycle sizes of the order of a typical stellar epicycle size where the amplitude of the oscillation in $\tilde{\kappa}$ has to be zero.

This article was processed by the author using Springer-Verlag TEX A&A macro package 1992.